Reactive MgO-based self-healing slag-cement-bentonite slurry walls

Benyi Cao[1, 2]* & Abir Al-Tabbaa[1]

Author 1 (corresponding author)

Benyi Cao, PhD, Research Associate, caobenyi@outlook.com

1. Department of Engineering, University of Cambridge, Civil Engineering Building, JJ Thomson Ave. 7a, Cambridge CB3 0FA, UK.

2. State Environmental Protection Key Laboratory of Soil Environmental Management and Pollution Control, Nanjing Institute of Environmental Sciences, Ministry of Ecology and Environment of China, Nanjing 210042, China.

Author 2

Abir Al-Tabbaa, PhD CEng FICE, Professor, aa22@cam.ac.uk

1. Department of Engineering, University of Cambridge, Civil Engineering Building, JJ Thomson Ave. 7a, Cambridge CB3 0FA, UK.

Abstract: Despite the common use of slag-cement-bentonite slurry trench walls for geotechnical and geoenvironmental applications, the materials deteriorate under mechanical, chemical and environmental stresses. Providing the slurry wall with the capacity of self-healing cracks, could address the concerns. This study proposes and investigates, for the first time, the self-healing slag-cement-bentonite incorporating reactive MgO pellets. The incorporation of the MgO pellets slightly increased the UCS and stiffness, without any significant adverse effects on the engineering properties of the slurry wall material. The crack closure percentages after hydration and carbonation reached over 50% and 80%, when the MgO pellets were added at a dosage of 5% and 10%. The post-healing permeability was as low as 8.4×10^{-9} m/s, satisfying the requirement for slurry walls. TGA and SEM-EDX results show that brucite and hydrated magnesium carbonates produced by the hydration and carbonation processes are the main healing products in the MgO-containing specimens. The uniform dispersion of MgO pellets and healing products was confirmed by micro-CT analysis, and it was observed most of the cracks could be at least partly blocked. The results have collectively demonstrated the great potential of reactive MgO pellets as an effective self-healing agent for the development of more reliable and resilient slag-cement-bentonite slurry walls.

Keywords: slag-cement-bentonite; slurry wall; self-healing; reactive MgO; microstructure.

Introduction

The cement-bentonite slurry trench wall is one of the most commonly used cut-off wall types [1], because they are adaptable and can be applied in the construction sites without suitable backfills or sufficient backfill mixing areas, or there are excessive slopes at the site [2]. The cement-bentonite slurry is prepared by mixing cement with a hydrated bentonite-water slurry just before its discharge into a trench. In traditional practice for cement-bentonite slurry walls, ordinary portland cement has been adopted as the main cementitious binder [3], [4]. Recently, ground granulated blast furnace slag (GGBS), produced from a by-product of the steelmaking industry, has become a more environmentally-friendly cement substitute [5], [6], [7]. Opdyke & Evans [8] investigated the effects of GGBS addition as cement replacement on the permeability and mechanical properties of cement-bentonite mixes. They found that when GGBS was added to replace 60% to 80% of cement, the unconfined compressive strength (UCS) and permeability of slag-cement-bentonite were improved significantly.

Despite the extensive use of cement-bentonite slurry walls for geotechnical and geoenvironmental applications, the slurry wall materials deteriorate under mechanical, chemical and environmental stresses [3], [9], [10], [11]. For example, vertical cracks with widths ranging from 0.5 to 1.5 mm were observed in the borehole sidewalls at the locations of field permeability tests during construction of a trench wall [9]. The crack surfaces were irregular and rough, and did not exhibit signs of shear distortion. It is therefore concluded that these cracks were attributed to drying shrinkage cracking. In

addition, a forensic investigation reported a case study of a cement-bentonite slurry trench wall failure due to the change in load in Australia [10]. The designed function of the cement-bentonite trench wall was to limit water ingress to an excavation site. However, as the excavation progressed the trench wall moved towards the excavation and the extent of this movement in the centre of the wall was noted to be up to approximately 300 mm, which led to cracking and failure of the wall.

The damage of cut-off walls can lead to the problems related to the undermined mechanical and transport properties, impacting their serviceability and reliability and in some cases leading to the undetected physical breach of the wall. For example, the relationship between the deformation response and permeability of slag-cement-bentonite was investigated by Alzayani [12]. The permeability immediately increased once the peak stress was exceeded (by 0.2% axial strain) to be 1.3×10^{-8} m/s compared with the permeability of 4.6×10^{-9} m/s for the intact samples. The permeabilities were highest at post-peak state when 2.2% axial strain was reached, and the values were between 10^{-6} and 10^{-7} m/s order of magnitudes.

Providing the slurry wall material with the capacity of self-healing cracks could significantly address such concerns [13]. The self-healing mechanisms of cementitious materials are generally classified into two categories: autogenous and autonomic. Autogenous healing is the innate healing capacity of cement-based materials to repair limited-width cracks (up to 0.15 mm and preferably less than 0.05 mm) [14]. The formation of calcite ($CaCO_3$) is the primary autogenous healing mechanism, under the

84 appropriate high-humidity curing conditions [15]. In contrast, the engineered
85 incorporation of materials capable of improving self-healing characterizes autonomic
86 healing, such as the incorporation of expansive minerals, microcapsules, and polymers
87 [16].
88 Reactive magnesia (MgO), an expansive mineral additive, has many merits, including
89 its chemically stable hydration product brucite, namely $Mg(OH)_2$, and relatively less
90 water requirement for the hydration [17], [18]. MgO can react with water to form
91 brucite ($Mg(OH)_2$) as shown in Equation 1. Brucite has a layered structure and its
92 morphology varies depending on the magnesium source and forming conditions [19].
93 $MgO + H_2O \rightarrow Mg(OH)_2$ (Brucite) Eq. 1
94 In the presence of water and CO_2, brucite can form one or more hydrated magnesium
95 carbonates (HMCs) [18], as shown in Equations 2-4.
96 $Mg(OH)_2 + CO_2 + 2H_2O \rightarrow MgCO_3 \cdot 3H_2O$ (nesquehonite) Eq. 2
97 $5Mg(OH)_2 + 4CO_2 + H_2O \rightarrow (Mg)_5(CO_3)_4(OH)_2 \cdot 5H_2O$ (dypingite) Eq. 3
98 $5Mg(OH)_2 + 4CO_2 \rightarrow (Mg)_5(CO_3)_4(OH)_2 \cdot 4H_2O$ (hydromagnesite) Eq. 4
99 These HMCs form ramified structure of large crystals with a high binding capacity,
100 resulting in significant and rapid strength increase [17].
101 The hydration of MgO and carbonation of brucite are both expansive reactions and the
102 increased solid volume could significantly fill the cracks and improve the self-healing
103 performance of cementitious materials. Qureshi and Al-Tabbaa [20] investigated the
104 ability of cement paste incorporating powder reactive MgO to self-heal the cracks

caused by drying shrinkage. They demonstrated that the crack surface area decreased by around 74-99% after a self-healing period of 56 days, which was much greater than the 43-79% reduction observed in control samples after in the same healing environment. Alghamri et al. [21] suggested to granulate powder reactive MgO and then encapsulate the MgO pellets using a spray coating technique to avoid pre-mature hydration of MgO during the mixing and curing period. Enhanced crack closure of the MgO-containing mortar samples was confirmed via microscopic inspection, and the incorporation of coated MgO pellets decreased the water capillary uptake by 30-65% compared to the control.

Collectively, these studies confirm that reactive MgO addition can contribute to producing healing products to fill and heal cracks of cement paste and mortar. Similar to autogenous healing, the presence of water is a prerequisite for the MgO-based self-healing mechanism. The main concern of the direct inclusion of MgO powder in the cementitious matrix is that when it is mixed with water, it might react immediately and be consumed prior to cracking. It is also of concern that the subsequent expansion of MgO in the interior matrix can occur, which could cause further cracks [22], [23]. Based on these previous studies, this study proposes and investigates, for the first time, the self-healing slag-cement-bentonite incorporating reactive MgO pellets. The proposed self-healing mechanism is shown in Figure 1. The compatibility of reactive MgO with the slurry system was investigated with regard to the variation in the fresh and hardened properties of slag-cement-bentonite. Self-healing efficacy was examined with regard to

crack closure and permeability recovery after hydration and carbonation. The self-healing processes and formation of self-healing products were revealed using scanning electron microscopy (SEM)-energy dispersive X-ray spectroscopy (EDX), thermogravimetric analysis (TGA) and micro-computed tomography (micro-CT). The results were discussed regarding the potential of the MgO-based self-healing approach to improve the performance of slag-cement-bentonite slurry walls.

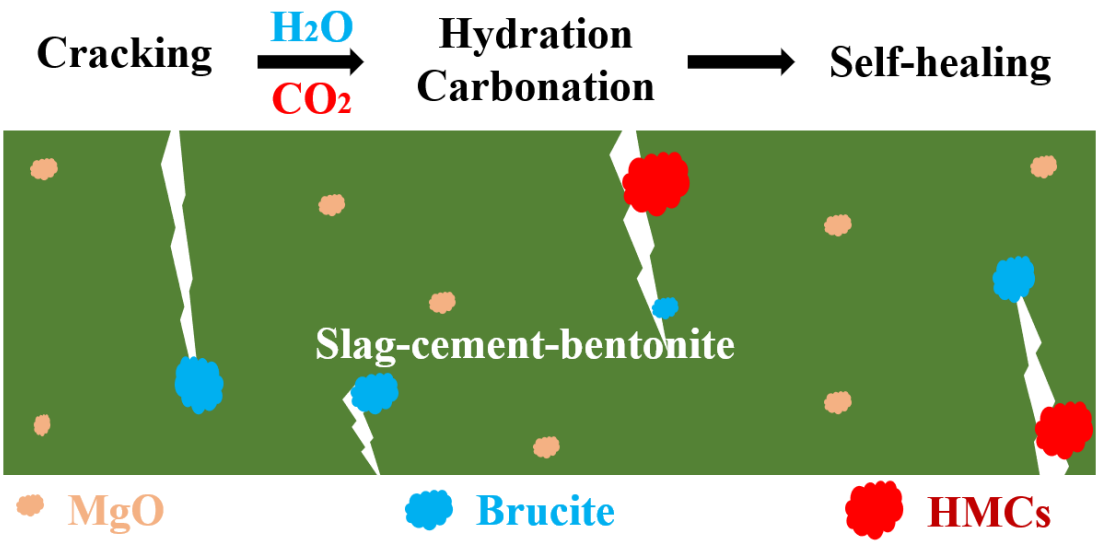

Figure 1. The proposed self-healing mechanism of slag-cement-bentonite incorporating reactive MgO pellets

Materials and methods

Slag-cement-bentonite and reactive MgO

A CEM I 52.5N Portland cement complying with BS EN 197-1, with a particle density of 2.7-3.2 g/cm^3, supplied by Hanson Limited, UK, was used. The ground granulated blast furnace slag (GGBS), which is a low-carbon and environmentally-friendly cement substitute, used in this study was Regen GGBS with a particle density of around 2.9 g/cm^3, manufactured from a by-product of the iron-making industry supplied by

Hanson Limited, UK. A sodium-activated bentonite produced to OCMA standard with a particle density of 2.4-2.6 g/cm^3 and a loss on ignition (LOI) of 8.6%, obtained from Macromin Kentish Minerals, UK, was used. Commercial reactive MgO pellets, LUVOMAG MO54 MgO, supplied by Lehmann & Voss, Germany, with the bulk density of 1850 kg/m^3 and particle sizes of 600-850 µm, were used (Figure 2). Principal oxides of the cement, GGBS, bentonite and reactive MgO pellets were summarized in Table 1.

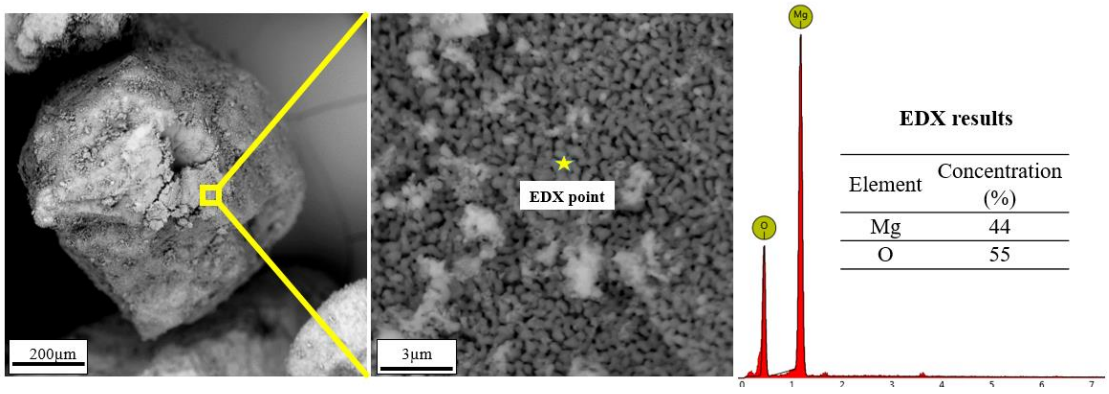

Figure 2. SEM images and EDX results of the MgO pellets used in this study

Table 1. Principal oxides compositions (%) of the cement, GGBS, bentonite and reactive MgO pellets used, as provided by the supplier.

	CaO	**SiO_2**	**Al_2O_3**	**MgO**	**Fe_2O_3**
Cement	65	20	5	1	2
GGBS	40	35	12	10	0.2
Bentonite	1.0	65.3	11.7	3.4	6.4
MgO pellet	3.0	3.0	0.3	90	0.7

Specimen preparation

All slag-cement-bentonite mixes were prepared using a Kenwood 1500W blender comprising of a stainless steel bowl and blade with a rotational speed of 190 rpm. The bentonite was first mixed with water for ten minutes to form a homogeneous bentonite slurry. The bentonite slurry was then left to hydrate for 24 hours, after which the dry cement, GGBS and MgO pellets were added. Ten cylinder specimens with a height of 100 mm and diameter of 50 mm and six disc specimens with a height of 10 mm and diameter of 50 mm were prepared for each mix. These specimens were left to cure in an incubator for 28 or 90 days at a temperature of 21 °C and 100% RH. Table 2 shows the mix constituents and nomenclatures.

Table 2. Mix composition (%) of slag-cement-bentonite slurry

Mix ID	**Slag-cement-bentonite slurry**				**MgO pellets (by**
	Bentonite	Cement	GGBS	Water	**total slurry weight)**
Control	5	4	16	75	0
MgO-5%	5	4	16	75	5
MgO-10%	5	4	16	75	10

Calorimetry, UCS and permeability tests

A Calmetrix I-Cal 2000 High Precision Isothermal Calorimeter compliant with ASTM C1679 was used to investigate the effects of MgO on the cement hydration process. The calorimeter recorded the heat flow rate during the hydration process to represent the reaction rate and calculated the cumulative heat evolution to represent the total degree of hydration. The incorporation of reactive MgO might alter the cement hydration process,

and the effect was quantitively analyzed.

The unconfined compressive strength (UCS) was determined in triplicate cylinder specimens based on ASTM: D4219-08 [24] using a Controls Testing Uniframe 70-T0108/E loading frame (Figure 3a). The UCS test was started by applying a constant axial displacement rate of 1.0 mm per minute until the peak force was reached. A linear variable differential transformer was used to determine the vertical displacement to calculate the axial strain.

The hydraulic conductivity of the cylinder specimens (Φ 50 x 100 mm) was measured using the flexible-wall method in triaxial cells according to ASTM: D5084-16 [25]. The cell pressure of 100 kPa was applied and maintained throughout the test. A water flow was applied via a peristaltic pump connected to the base and the water flowed to the top of the cylinder specimens. A pore pressure transducer was connected to the inflow pipe to measure the pressure built and the value was recorded continuously (Figure 3b). The first permeability tests were conducted on the undamaged specimens after 28-day curing, after which the specimens were cracked using the UCS testing frame. The compressive load was removed from the specimen immediately when the peak force was reached; in this way cracks with a width of 0.05-0.25 mm were obtained. The second permeability tests were carried out on the day of cracking, and then the cracked specimens were returned to the incubator for a period of self-healing before the third permeability tests on the post-healing specimens.

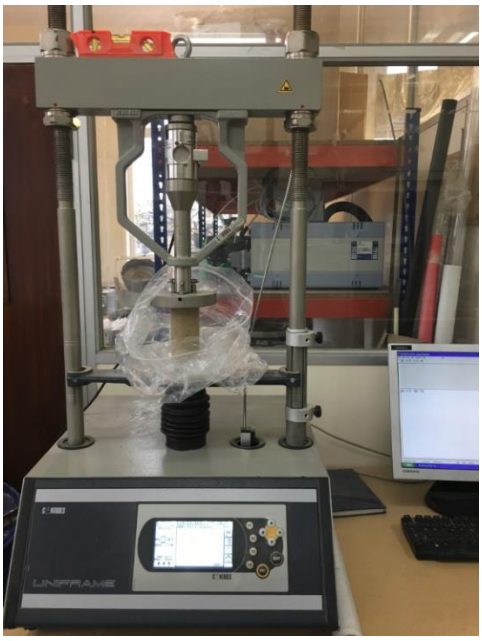

(a)

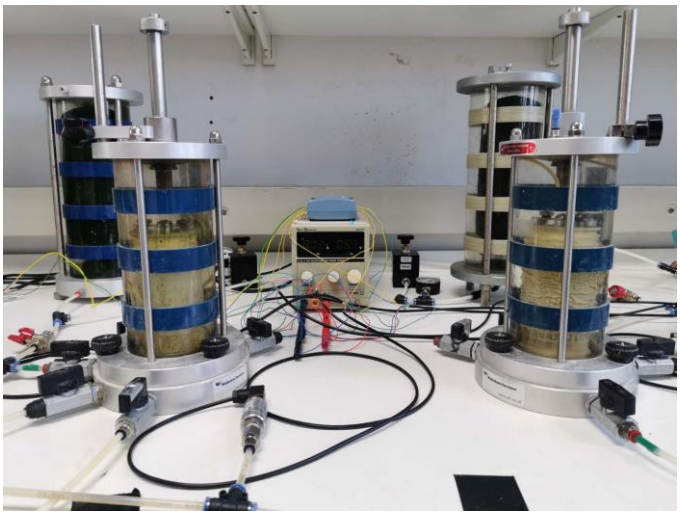

(b)

Figure 3. (a) Specimen tested by Uniframe 70-T0108/E Control Machine; (b) the permeability test setup.

Surface crack analysis

Optical microscopy (Leica LED2000) was used for the surface crack analysis of the slag-cement-bentonite specimens. The disc specimens (Φ 50 x 10 mm) were cracked in

splitting tests using the compression frame and the load was removed from the specimen edge immediately when the peak force was reached; in this way cracks with a width of 0.05-0.25 mm and depth of 10 mm were obtained. The two-step volumetric expansion of MgO, i.e., the hydration of MgO and carbonation of brucite, can happen to heal the crack. To facilitate the two-step volumetric expansion of MgO, a two-step healing method was adopted in this study. First, the cracked disc specimens were submerged in a water tank to hydrate the MgO pellets on the crack surfaces for 28 days to yield brucite. Next, these hydrated specimens were healed in a CO_2 incubator with a 20% CO_2 concentration for another 14 days to yield HMCs. High-concentration CO_2 curing has been suggested and commonly used to accelerate the carbonation of cement-based products and facilitate carbon sequestration in solid mineral phases [26]. Optical microscope images were taken on the day of cracking, after 28-day hydration and after 14-day carbonation in several locations (e.g. 10 spots) along the crack, and image analysis software was used to calculate the average crack width.

Microstructural tests

Phenom Pro X SEM was used to characterize the microstructural surface morphology of the sample with MgO and EDX was used to analyze the elemental composition. Small chips extracted from the cracked and post-healing slag-cement-bentonite specimens were vacuum dried at 20 °C for 24 hours before being scanned, and images were captured at different magnifications.

TGA tests of extracted cementitious particles were carried out using a Perkin Elmer

STA 6000. The variation of sample weight with temperature with precision during the heating process was measured and recorded. Small amounts of the extracted sample (10±2 mg) from the cracked and post-healing specimens were placed into a ceramic crucible. The sample was then heated up from 30 to 1000°C at a constant rate of 10 ℃/min. Thermogravimetric and the first derivative of the thermogravimetric (DTG) curves were obtained by plotting normalized sample weight with temperature.

Micro-CT scan produces a 3D distribution of the local linear attenuation coefficient in the form of grey values, and specialized rendering software (VGStudio MAX) allows for image analysis of this 3D volume. Cubic slag-cement-bentonite samples, around $10\times10\times10$ mm^3, were cut carefully from the disc specimens using a blade and scanned using Nikon XT H 225 ST. A flat panel detector with 2000×2000 pixel was used and the four test parameters were set as follows: (i) X-ray energy: 70 kV mA, which are parameters determined by the sample geometry and the material composition; (ii) geometric magnification ratio: 39.5; (iii) reconstructed image matrix volume: 2000×2000×1000 voxels and (iv) effective voxel size: 5.05 μm. A subsample cuboid region of interest was then extracted for ease of analysis, and the Gaussian filter was applied to remove image noise and improve the quality. Image segmentation was then carried out to separate the digital image into multiple phases based on the difference in grey values of each phase.

Results and discussion

Effects of MgO pellets on slag-cement-bentonite properties

Hydration of cement

The effects of MgO addition were investigated on the hydration process of slag-cement-bentonite slurry. If the MgO pellets are already completely hydrated during the mixing and curing period, they would fail to expand and block the cracks when cracking occurs. In that case, it would be necessary to coat these MgO pellets with a film before mixing to prevent premature hydration of MgO. In literature, polyvinyl alcohol-based film coatings have been proposed to encapsulate several expansive pellets to prevent premature consumption and uncontrolled reactivity in contact with water for the development of self-healing mortar [27], [28].

The heat flow curves of the slag-cement-bentonite samples containing different dosages of MgO pellets, in comparison to the control for the first 24 hours were recorded and shown in Figure 4. The addition of the MgO pellets up to 10% by total slurry weight only slightly delayed the peak power time by around 0.5 hour. Portlandite nucleation theory has been among the most acknowledged explanations of the induction periods of cement hydration. When calcium cations and hydroxide anions reach their maximum supersaturation state and start to nucleate and precipitate the induction of cement hydration finishes [29]. For the MgO-based slag-cement-bentonite mixes, the Ca^{2+} and OH^- ions are produced by cementitious binders (cement and GGBS) and Mg^{2+} and OH^- ions are also released by the much slower hydration of reactive MgO pellets before reaching supersaturation. Despite the slower release of Mg^{2+}, brucite nucleates and precipitates earlier than portlandite thanks to its much smaller solubility. As a result,

hydroxide anions are consumed for the formation of brucite, which leads to a decrease in the OH^- concentration. The supersaturation of portlandite is therefore delayed and the cement hydration induction is prolonged. It should also be noted that the retardation effect was very slight, indicating that only a very small amount of MgO was hydrated during the curing period. This is because the $Mg(OH)_2$ produced during the early induction stage precipitates fast on the surface of the MgO pellets, creating a brucite coat and preventing further hydration of the inner MgO pellets. It was considered, therefore, unnecessary to coat the MgO pellets with a PVA film.

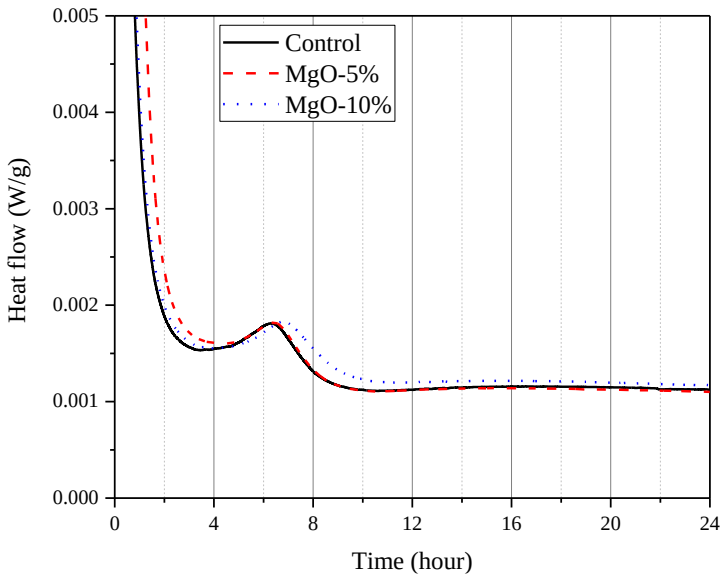

Figure 4. The variation of heat flow with cement hydration time

Mechanical properties

The values of UCS and strain at failure were measured after 28 and 90 days of curing. Figure 5(a) showed that the addition of MgO pellets generally increased the UCS. For example, the UCS of MgO- 5% and MgO-10% were 13% and 18% higher than the control value of 733 kPa after 28 days of curing. A similar trend was observed on day

90, although the gap between the control and MgO-containing specimens narrowed. The main reason for the UCS increase was because the added MgO pellets acted as fine aggregates to provide compressive strength in the slag-cement-bentonite mixes. As a result of the addition of hard aggregates, the specimens became stiffer, and the strain at failure decreased slightly (Figure 5b). The strain at failure of the control was 1.5% after 28-day curing, and the value decreased to 1.3% and 1.1% when the MgO pellets were added at 5% and 10% by total slurry weight. An overall stress-strain response of the slag-cement-bentonite mixes after 28-day curing is revealed in Figure 5(c). In general, the stiffness increased with the increasing dosage of the added MgO pellets, with a higher peak stress and a lower peak strain. However, the addition of the MgO pellets failed to alter the failure mode. All the specimens show a tensile failure mode with a major vertical crack along the generatrix of the cylinder specimens. Therefore, the addition of the MgO pellets only slightly increased the UCS and stiffness, without any significant adverse effects.

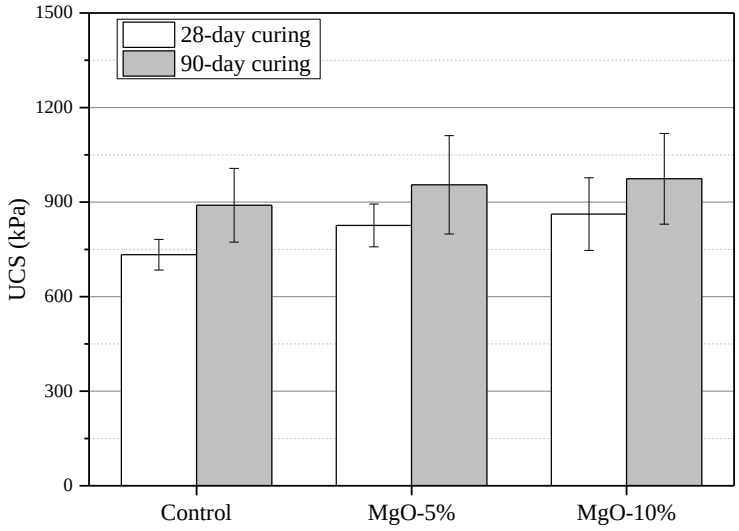

(a)

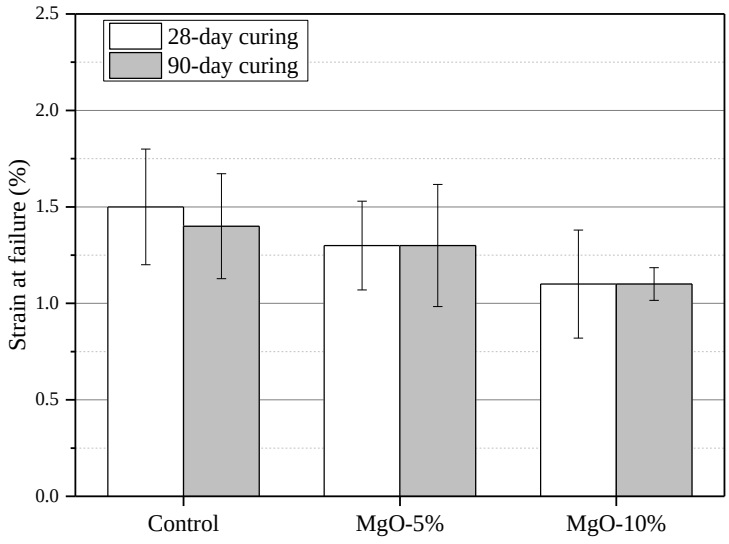

(b)

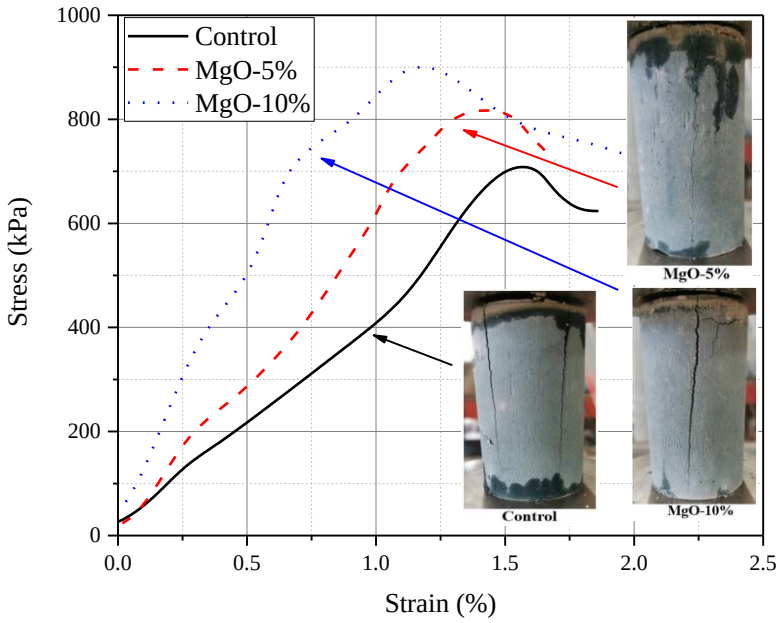

(c)

Figure 5. The (a) UCS, (b) strain at failure and (c) 28-day stress-strain curves of the slag-cement-bentonite specimens with different MgO pellets dosages

Self-healing performance

Crack closure

In order to examine the ability of the MgO pellets to heal cracks, optical microscope images were taken on the surface of slag-cement-bentonite disc specimens after different self-healing periods. The crack closure percentage is a convenient and important indicator of self-healing performance for cementitious materials [16]. Upon reaching the peak stress under the UCS frame, the disc specimens had residual crack widths in the range of 300-600 μm. In literature, it has been shown that the autogenous healing of cementitious materials is usually limited to tight crack widths up to 150 μm and preferably less than 50 μm [14]. Therefore, the wide cracks induced here were supposed to be very challenging for autogenous self-healing, so that the autonomic healing due to the MgO pellets can be highlighted if significant crack closure can be observed.

The development of healing products on the surfaces of typical cracked specimens was illustrated in Figure 6(a). On the control specimen, only a very small amount of healing product was found on the edge of the cracks. The formation of calcium carbonates is believed to contribute mainly to the limited autogenous self-healing [30]. In contrast, plenty of healing products (mainly brucite) were observed on MgO-5% and MgO-10% after 28 days of hydration, and even more (mainly HMCs) were found after further 14-day carbonation. Some parts of the cracks on MgO-containing specimens were even completely healed by the healing products. This indicates that the MgO pellets embedded in slag-cement-bentonite survived the mixing and curing period, and were successfully hydrated and carbonated to yield expansive minerals to heal the cracks.

To quantify the crack healing, the crack closure percentage was calculated after the two healing steps using Equation 5.

$$\text{Crack closure percentage (\%)} = \left(1 - \frac{W_{post-healing}}{W_{initial}}\right) \times 100\% \quad \text{Equation 5}$$

where $W_{\text{post-healing}}$ is the crack width after a self-healing period, and W_{initial} is the crack width on the day of cracking. A crack closure percentage of 100% means that the crack is completely healed. The crack closure percentages after 28-day hydration and 14-day carbonation were presented in Figure 6(b). Confirming the microscope observations, the addition of the MgO pellets resulted in a significant improvement in crack closure percentage compared to the control. Only less than 10% crack closure was observed for the control, suggesting the autogenous self-healing in slag-cement-bentonite was very limited. In contrast, the crack closure percentages after hydration and carbonation reached over 50% and 80%, when the MgO pellets were added at a dosage of 5% and 10%, respectively.

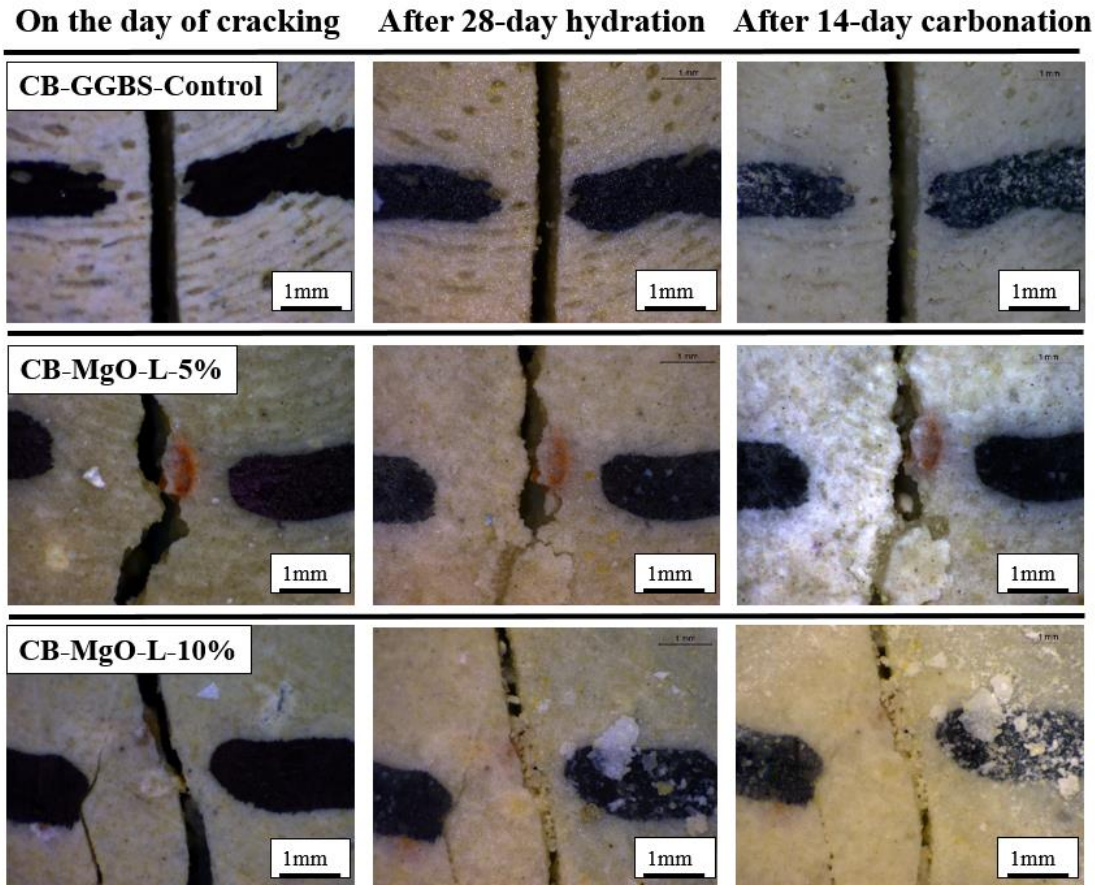

(a)

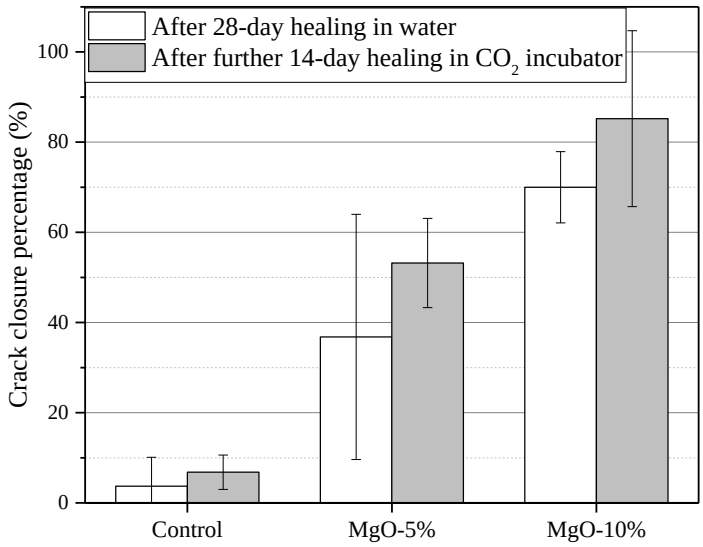

(b)

Figure 6. Crack closure of slag-cement-bentonite after 28-day hydration and 14-day carbonation: (a) representative images of cracks and (b) crack closure percentage.

Recovery of permeability

The recovery of permeability was investigated for a thorough assessment of self-healing performance. Figure 7 shows the results of the permeability tests on the undamaged specimens, as well as their cracked and post-healing counterparts. Generally, the incorporation of the MgO pellets had a negligible effect on the permeability of undamaged slag-cement-bentonite after 28-day curing. The permeabilities of MgO-5% and MgO-10% were 5.24×10^{-9} m/s and 4.33×10^{-9} m/s compared with the control value of 6.01×10^{-9} m/s. This means the MgO pellets had a good bonding with the cementitious matrix and no flow channels were created due to the incorporation of the MgO pellets. After cracking using the UCS frame, the damaged control, MgO-5% and MgO-10% specimens had similar permeabilities of 7.5×10^{-8}, 1.1×10^{-7} and 1.2×10^{-7} m/s, all of which were higher than the undamaged values by over an order of magnitude. After the period of self-healing, the MgO pellets on the crack surfaces reacted with water and CO_2 and yield expansive brucite and HMCs, thus decreasing the permeability. The permeabilities of post-healing MgO-5% and MgO-10% dropped to 1.7×10^{-8} and 8.4×10^{-9} m/s due to the conversion of the MgO into healing products. This indicates that the expansive healing products created by the MgO pellets recovered the water-tightness substantially. It was obvious that a higher dosage of MgO pellets could yield more brucite and HMCs to heal the cracks, and therefore the recovery of permeability was more significant. The pronounced reduction in permeability was in good agreement with the crack closure results obtained in the previous section. Bureau of Reclamation

[31] specified a permeability of 1×10^{-8} m/s to be expected in the finished cut-off wall. The recovered permeability of MgO-10% was less than 1×10^{-8} m/s, which indicates the post-healing MgO-containing specimens can satisfy the permeability requirements for a cut-off wall. In contrast, the permeability of post-healing specimens of control mix shows almost no recovery, indicating very limited autogenous healing. Although it is well known that bentonite will expand when contacting water, studies have shown that bentonite clay minerals dissolve in slag-cement-bentonite slurries and that bentonite is virtually absent in the hardened mix, thus contributing little to self-healing [32]. Overall, these findings are a strong indication that the recovery of permeability of slag-cement-bentonite can be substantially improved by incorporating reactive MgO pellets.

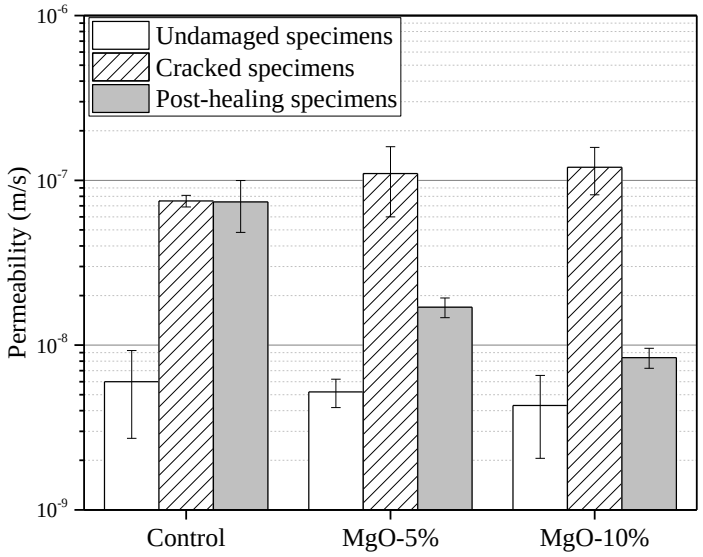

Figure 7. The permeabilities of undamaged, cracked and post-healing slag-cement-bentonite specimens

Microstructural analysis

Characterization of healing products using TGA

TGA tests were used to analyze the healing products on the crack surfaces after the 28-day hydration and 14-day carbonation periods. For slag-cement-bentonite mixes, the weight loss from 100 to 300 °C could be ascribed to the evaporation of the physically adsorbed water and bound water from the HMCs and CSH gel layers. The mass loss from 300 to 400 °C corresponded to the dehydroxylation of $Mg(OH)_2$ and partly decarbonization of HMCs. The mass drop at higher temperatures (from 450 to 600 °C) was associated with the decomposition of metastable Mg/Ca-carbonates, and the mass loss at temperatures above 600 °C mainly resulted from the decomposition of stable and well-crystallized $MgCO_3$ and $CaCO_3$ [33]. However, CSH itself shows weight loss over a broad range of temperatures; particularly between 50 and 600 °C. Quantification of CSH by measuring the change in mass between these temperatures, therefore, is not reasonable as most other hydrates show their characteristic signals in this range [34].

The mass loss and DTG curves of the undamaged samples after 28-day curing are shown in Figure 8(a&b), and those of post-healing samples after 28-day hydration and 14-day carbonation are in Figure 8(c&d). The TGA temperature ranges, and corresponding weight losses at each step are presented in Table 3. In the undamaged control samples, clear endothermic peaks at 400 and 725 °C are detected, corresponding to the decomposition of portlandite and calcite. In contrast, much higher peaks at similar temperatures are detected in MgO-containing samples, indicating that brucite and HMCs existed in the samples due to the slight hydration and carbonation of the MgO pellets during the mixing and curing periods. The weight losses between 300-450 °C of

398 the undamaged MgO-5% and MgO-10% were 5.1% and 7.3%, respectively, compared
399 with the control value of 2.6%. This is because the increasing dosage of MgO pellets
400 increased the brucite content.
401 In post-healing samples, the intensity of the peaks between 300 and 450 °C drastically
402 decreased for all samples due to the 14-day carbonation. After the self-healing period,
403 the portlandite in the control samples was carbonated to yield calcite, and the mass loss
404 resulting from calcite decomposition almost doubled compared with the undamaged
405 ones. The conversion of portlandite into calcite was believed to be the main factor
406 contributing to the autogenous self-healing process [15]. This begins by the leaching of
407 soluble calcium ions from the bulk slag-cement-bentonite matrix into cracks. In the
408 presence of water and dissolved CO_2, Ca^{2+} will crystallize to create $CaCO_3$ on the crack
409 surface, which was also widely reported in the literature [14], [35]. In contrast, the
410 brucite and HMCs due to the hydration and carbonation of MgO pellets were the main
411 healing products in the MgO-containing samples. Clear peaks corresponding to brucite
412 could still be observed because the continuously generated brucite was not completely
413 carbonated during the self-healing period. This means that the healing capacity of the
414 added MgO pellets was not thoroughly exploited, which is beneficial as the unhydrated
415 MgO could be used for future self-healing if cracking occurs again. The weight losses
416 between 450-900℃ of the post-healing MgO-5% and MgO-10% were 24.7% and
417 25.6%, respectively, compared with the control value of 20.5%. Some brucite was
418 successfully converted into HMCs, resulting in an increase in the HMCs content of the

post-healing samples. It should also be noted that, in the post-healing control samples, the ratio of carbonates/hydroxides was 13.6; however, the ratios decreased to 4.2 and 4.6 for MgO-5% and MgO-10%, respectively. This indicated that the main autogenous healing product in the control samples was calcite, whereas both brucite and HMCs contributed greatly to the autonomic healing of MgO-containing samples.

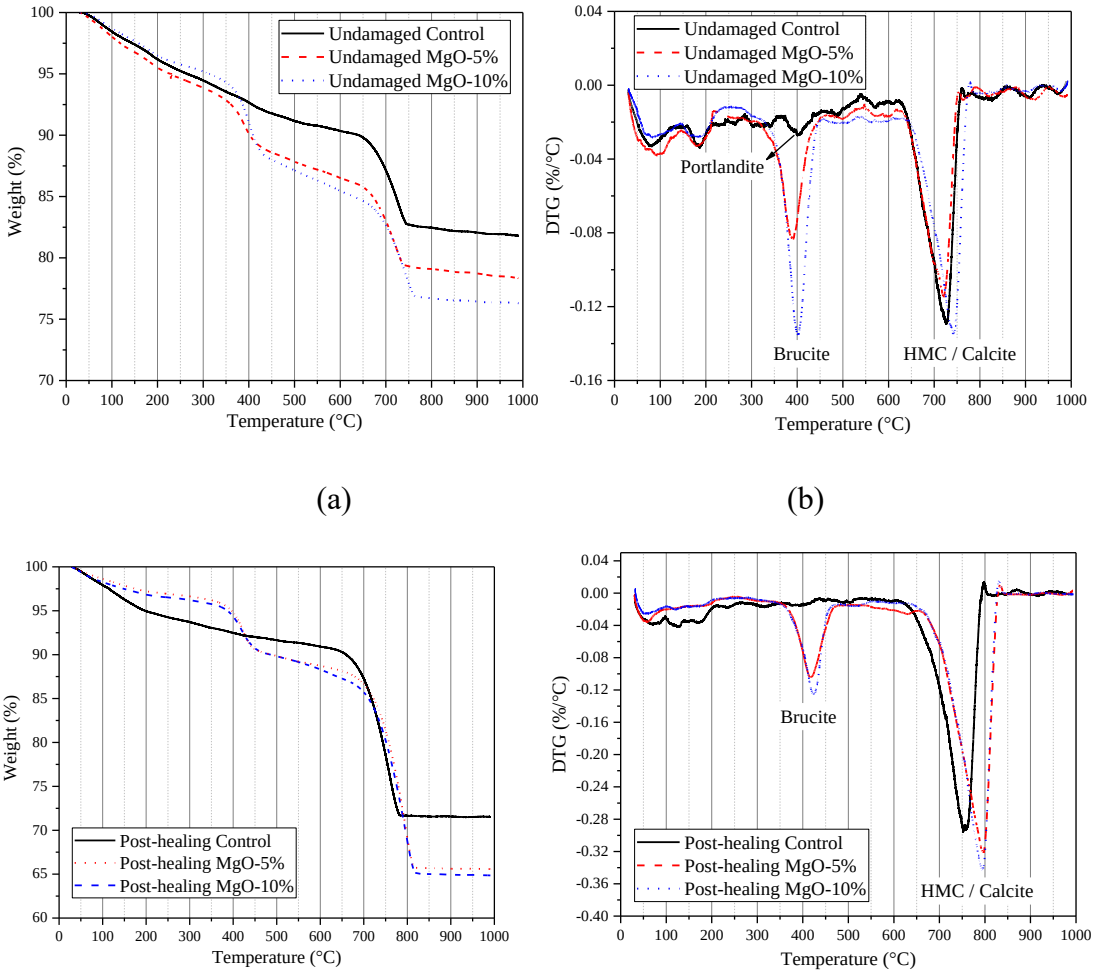

Figure 8. (a) Mass loss and (b) DTG curves of undamaged slag-cement-bentonite; (c) mass loss and (d) DTG curves of post-healing slag-cement-bentonite after 28-day hydration and 14-day carbonation

Table 3. TGA mass loss of undamaged and post-healing slag-cement-bentonite

Sample	Mass loss (%)		
	50-300°C	300-450°C	450-900°C
Undamaged Control	5.5	2.6	9.8
Undamaged MgO-5%	6.3	5.1	9.9
Undamaged MgO-10%	4.8	7.3	11.4
Post-healing Control	6.4	1.5	20.5
Post-healing MgO-5%	3.3	5.8	24.7
Post-healing MgO-10%	3.8	5.6	25.6

Morphology analysis using SEM-EDX

The representative SEM images and EDX results of the MgO-10% sample after 28-day curing are shown in Figure 9. The MgO pellets could be clearly identified in the cementitious matrix, and some cement hydration products precipitated on the surface of the pellets, indicating fairly good bonding between the MgO pellets and the matrix. A zoomed-in image on the surface of the MgO pellet showed the morphology of the brucite and dypingite/hydromagnesite yielded as a result of the slight hydration and carbonation of MgO. Brucite occurred as single disks made of layers of hexagonal flakes, and hydromagnesite/dypingite as rosette clusters with flower-like morphologies of variably spaced flaky crystals [36], [37]. EDX analysis was conducted at two points on the surface of the MgO pellet. The primary elements detected were Mg, O, and Ca. The elemental ratio of O/Mg was 2.3 at EDX-1 point, and 2.5 at EDX-2 point. The

elemental ratio of O-to-Mg of the hydration and carbonation products of MgO is 2.0 for brucite ($Mg(OH)_2$), 3.6 for hydromagnesite ($4MgCO_3 \cdot Mg(OH)_2 \cdot 4H_2O$), 3.8 for dypingite ($4MgCO_3 \cdot Mg(OH)_2 \cdot 5H_2O$), and 6 for nesquehonite ($MgCO_3 \cdot 3H_2O$). Based on the detected O/Mg ratio (2.3-2.5), the minerals observed on the surface of the MgO pellet after 28-day curing were, therefore, mainly brucite, with a small amount of dypingite/hydromagnesite. Similar microstructural makeup was reported by Alghamri & Al-Tabbaa [27] and Dung & Unluer [38]. This confirmed the findings of the TGA tests that the MgO on the surface of the pellets was partly hydrated and carbonated during the mixing and curing processes.

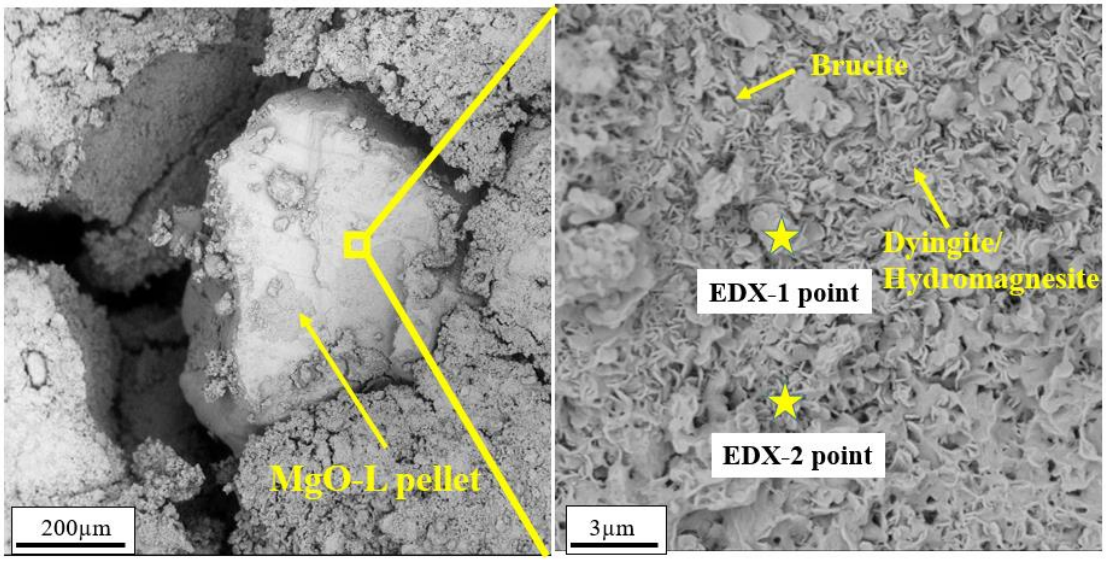

(a)

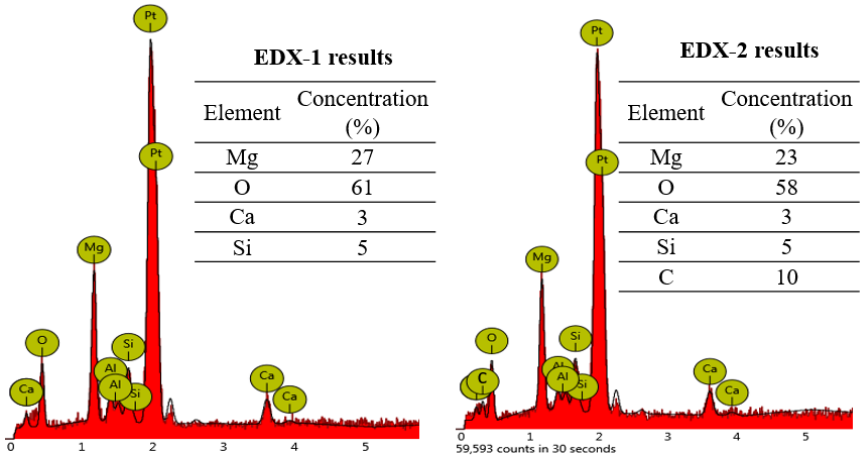

(b)

Figure 9. (a) Representative SEM images and (b) EDX results of the MgO-10% sample after 28-day curing

The results of the second SEM-EDX tests carried out on the post-healing sample that was hydrated for 28 days and carbonated for 14 days after cracking are shown in Figure 10. Overall, these observations verified the TGA results and confirmed the contribution of the hydration and carbonation of the MgO pellets to the formation of the healing products. On the crack surface, the abundant formation of clusters of rosette-like hydromagnesite/dypingite is observed, mixed with nesquehonite exhibited variably sized, elongated strip-shaped crystals. The EDX results on the crack surface showed an O/Mg ratio of 6.7 for EDX-3 point and 5.6 for EDX-4 point. Compared with the O/Mg ratio of 2.3-2.5 for the pre-healing sample in Figure 9, the O/Mg ratio of the post-healing sample almost tripled. This indicated that the MgO pellets were mainly converted into oxygen-rich carbonates including hydromagnesite, dypingite and nesquehonite after the self-healing period. The detected O/Mg ratios of 5.6-6.7 were

very close to the O/Mg ratio of nesquehonite (6.0), suggesting the main healing product was nesquehonite. The observation is in good agreement with Wang et al. [33], where nesquehonite was found to be the most prominent Mg carbonate phase during flow-through CO_2 curing. It is known that nesquehonite is a metastable compound that can transform into less hydrated forms (dypingite/hydromagnesite) depending on the conditions it is exposed to, including changes in temperature, CO_2 partial pressure, pH and water activity [39]. As a result, the nesquehonite formed in the post-healing sample could gradually transform into dypingite or hydromagnesite in the long run. In previous research looking into the carbonation of MgO systems at room temperature, the three main forms of HMCs usually co-exist in the same mixes [40].

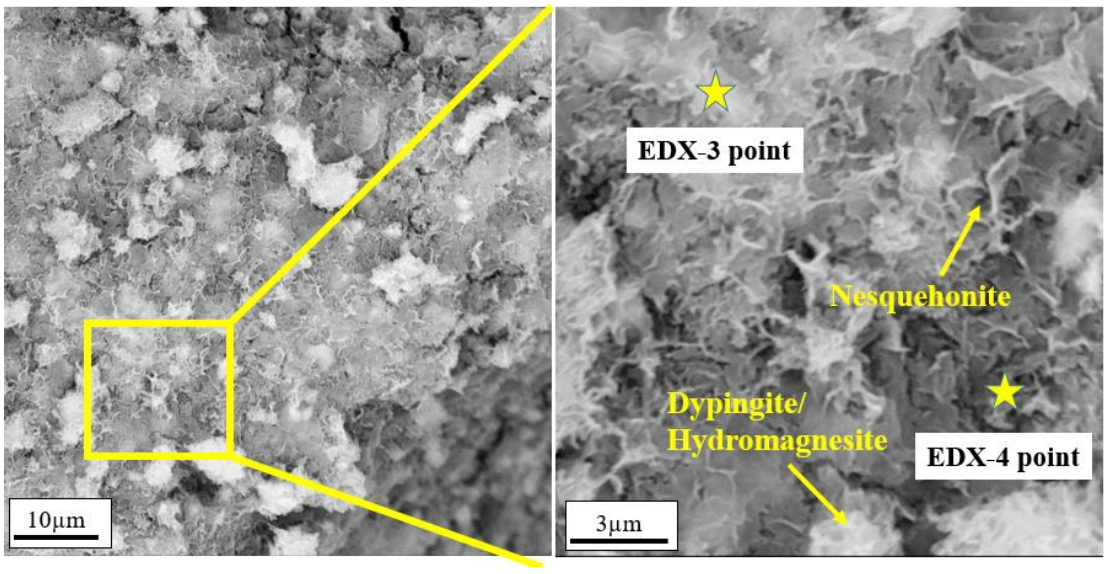

(a)

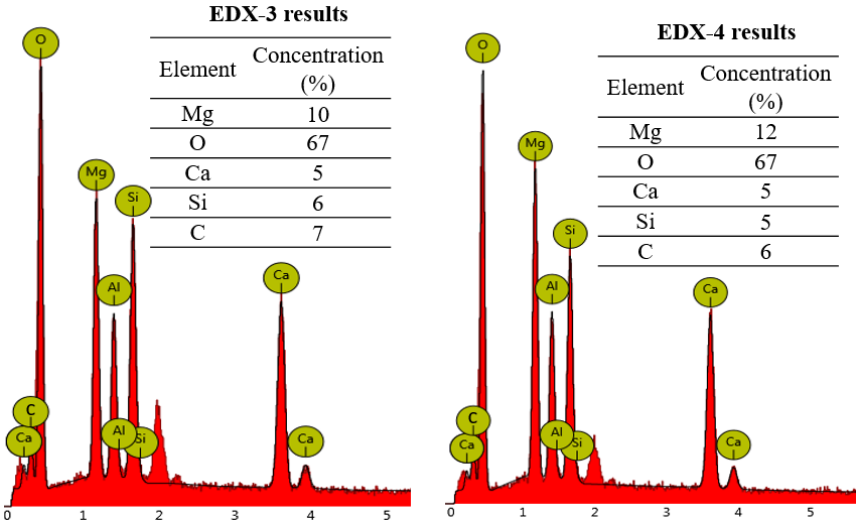

(b)

Figure 10. (a) Representative images and (b) EDX results of the post-healing MgO-10% sample after 28-day hydration and 14-day carbonation

3D microstructural analysis using Micro-CT

High-resolution X-ray micro-computed tomography was conducted on the undamaged, cracked and post-healing MgO-10% sample to investigate the 3D distribution and microstructure of the MgO pellets and healing products. As shown in Figure 11, the reconstructed images of the undamaged sample contained two phases: (1) the light phase of slag-cement-bentonite matrix in olive color, and (2) the dense phase of MgO pellets in orange color. The void sizes in the specimens are too small to be analysed, and therefore air space was ignored as image noise by applying Gaussian filter. In the 2D cross-sections, the MgO pellets were seen to be uniformly distributed over the slice, suggesting the good survivability and dispersion of the MgO pellets during the mixing process.

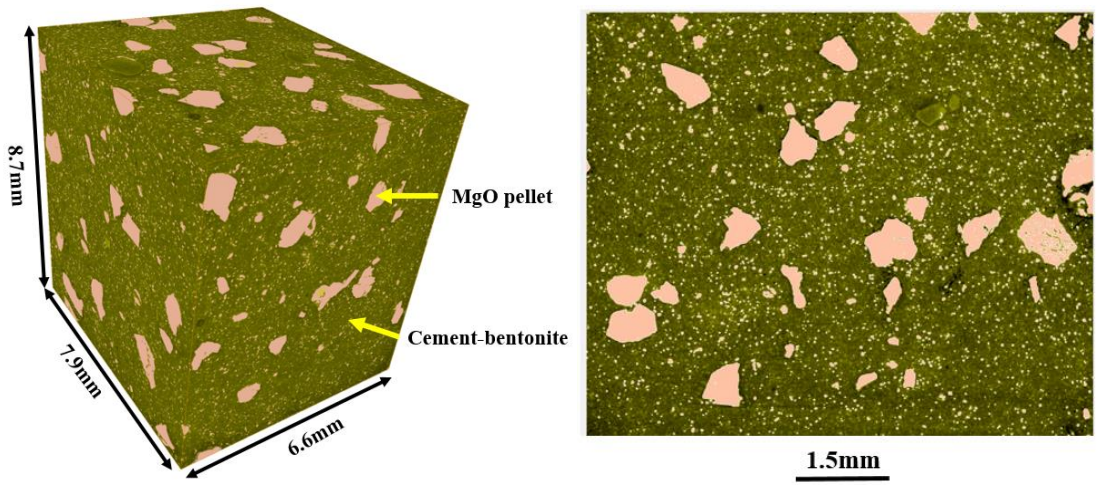

(a) (b)

Figure 11. (a) 3D and (b) 2D image of an undamaged MgO-10% sample (orange - MgO pellets, and olive – slag-cement-bentonite)

To introduce cracks, the cubical sample was air-dried in the standard lab environment for 24 hours and the desiccated and cracked sample was scanned for the second time (Figure 12). From the reconstructed images, cracks shown in black with an average width of 284±103μm were randomly distributed over the sample. The uniform distribution of the MgO pellets in the matrix increased the possibility of the cracks intersecting the MgO pellets. As a result, the majority of the MgO pellets were exposed to crack surfaces, which can facilitate the hydration and carbonation reactions in the self-healing period.

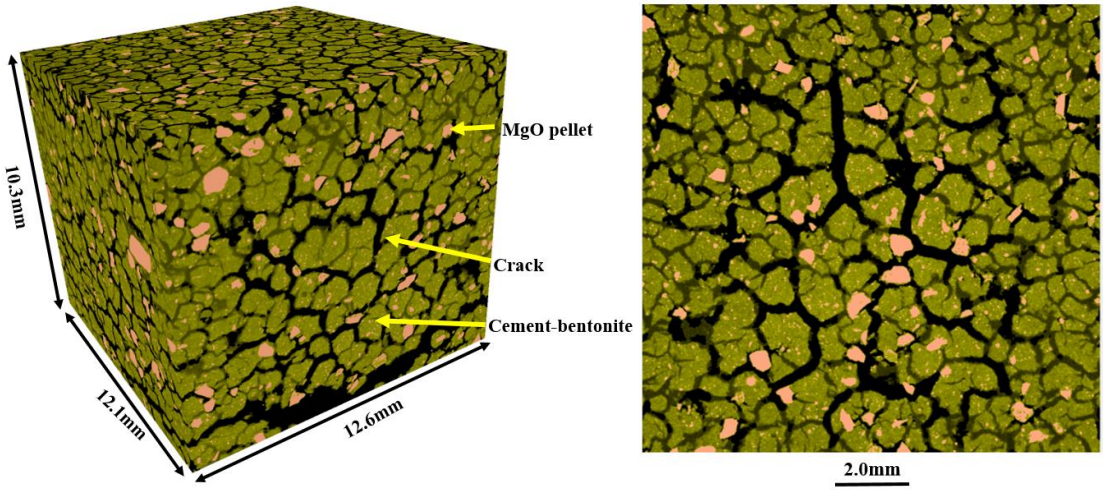

(a) (b)

Figure 12. (a) 3D and (b) 2D image of the cracked MgO-10% (black - cracks, orange - MgO pellets, and olive - slag-cement-bentonite)

The post-healing MgO-10% sample was scanned for the third time after the 28-day hydration and 14-day carbonation periods as shown in Figure 13(a&b). The reconstructed images contained four phases: (1) the lightest phase of crack in black, (2) light phase the slag cement-bentonite (1.2 g/cm^3) in olive, (3) the dense phase of brucite and HMCs (2.4-2.9 g/cm^3) in purple, and (4) the densest phase of MgO (3.6 g/cm^3) in orange. Compared with the cracked one, abundant healing products (brucite and HMCs) with a slightly lower density than the MgO pellets were found in the cracks. These healing products were colored purple in the reconstructed images. Segmentation analysis shows that around 17% of the total crack volume was occupied by these healing products. It is shown that many of the cracks, especially the cracks with a smaller width, were effectively blocked by the yielded healing products. Based on the results of TGA and SEM-EDX tests, these healing products are believed to be mainly

HMCs. The MgO pellets and healing products were extracted from the cementitious matrix and shown in Figure 13(c). Similar to the dispersion of the MgO pellets, the distribution of the healing products was also uniform in the matrix. This means most of the cracks could be at least partly blocked, preventing the formation of connected channels for preferential flow. In such way, the permeability was reduced and the MgO-containing samples self-healed once the expansive HMCs were formed during the healing period. In general, the observations from the micro-CT scan confirmed the uniform dispersion of the MgO pellets and effective blockage of cracks by the HMCs formed during the hydration and carbonation self-healing period. It should be noted that the self-healing performance was investigated after 28-day hydration and 14-day carbonation of MgO. Further expansion of MgO could happen after the 42 days and more crack volume might be sealed by healing products. The expansion of MgO will stop when the cracks and voids are completely blocked as water and CO_2 cannot come into contact with the MgO particles. Therefore, it is unlikely that the further expansion of MgO will cause significant internal stress and additional cracks and damage to the cementitious matrix.

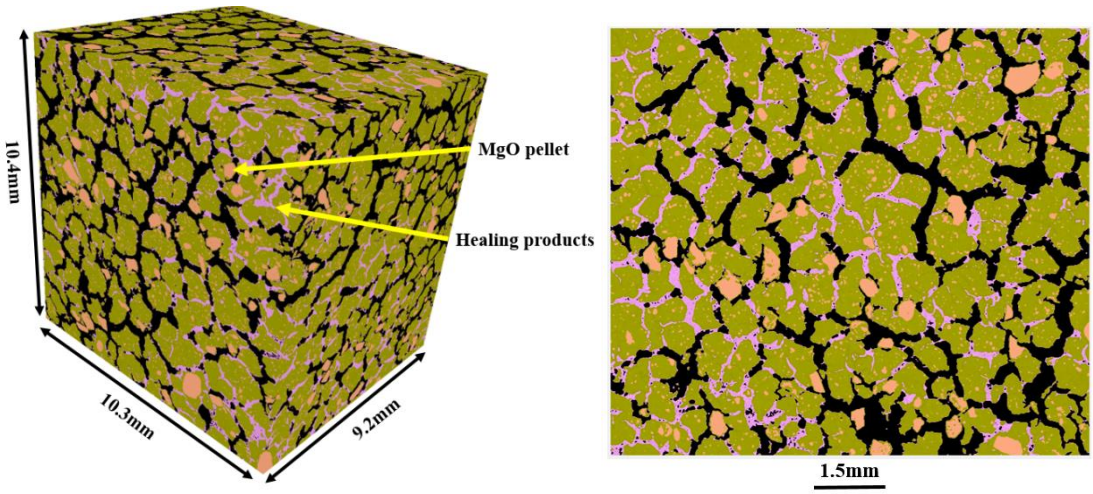

542

543 (a) (b)

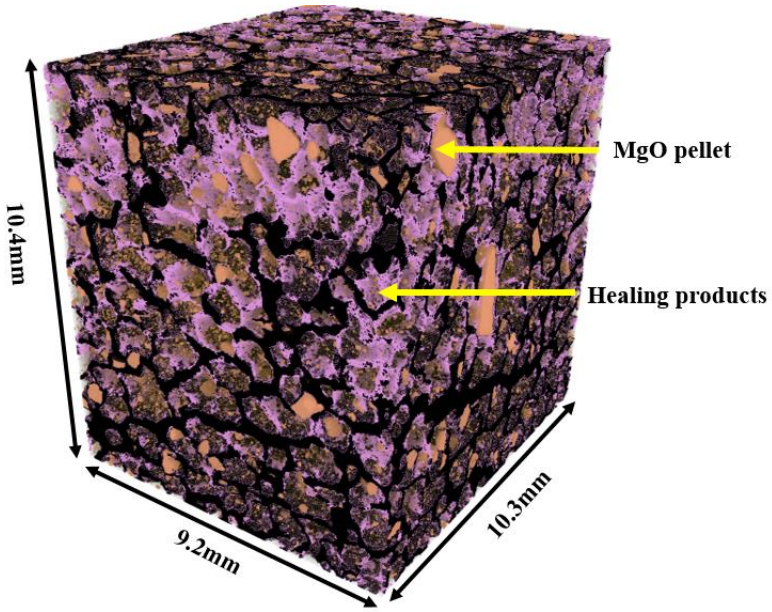

544

545 (c)

546 Figure 13. (a) 3D and (b) 2D images of the post-healing MgO-10% (black - cracks,

547 orange - MgO pellets, olive - slag-cement-bentonite, and purple - healing products);

548 (c) extracted MgO pellets and healing products

549 # Conclusions

550 This study investigates the performance of reactive MgO-based self-healing slag-

551 cement-bentonite slurry wall material. Lab testing to assess the effects of MgO pellets

addition and the self-healing performance of the slag-cement-bentonite found:

- The retardation effect of MgO pellets on cement hydration was very slight, indicating the pellets survived the mixing and curing period and that it was unnecessary to coat the MgO pellets.
- The addition of the MgO pellets only slightly increased the UCS and stiffness, without any significant adverse effects on the engineering properties of the slurry wall material.
- The crack closure percentages after hydration and carbonation reached over 50% and 80%, when the MgO pellets were added at a dosage of 5% and 10%, respectively. The post-healing permeability of MgO-10% was 8.4×10^{-9} m/s, satisfying the permeability requirement for a slurry wall.
- TGA revealed that brucite and HMCs due to the hydration and carbonation of MgO pellets were the main healing products in the MgO-containing samples, which was further verified by SEM-EDX analysis.
- The uniform dispersion of MgO pellets and healing products was confirmed by micro-CT analysis, and it was observed most of the cracks could be at least partly blocked, preventing the formation of connected channels in the slurry material.
- The results collectively demonstrated the significant potential of reactive MgO pellets as a self-healing approach for the development of more resilient slag-cement-bentonite slurry walls.

Data Availability Statement

All data, models, and code generated or used during the study appear in the submitted article.

Acknowledgement

This research was funded by the EPSRC program grant Resilient Materials for Life

577 (RM4L) (EP/P02081X/1) and the Youth Program of National Natural Science
578 Foundation of China (42107220).

579 References

580 [1] Jefferis, S. (1997). The origins of the slurry trench cut-off and a review of cement-
581 bentonite cut-off walls in the U.K. Proc., Int. Containment Technology Conf., 52-70.
582 [2] Hodge, V, Robinson, T, Spooner, P, Wetzel, R, Spooner, C, Furman, C, Tokarski, E,
583 & Hunt, G. (1985) Slurry trench construction for pollution migration control. United
584 States.
585 [3] Garvin, S. L., & Hayles, C. S. (1999). The chemical compatibility of cement–
586 bentonite cut-off wall material. Construction and Building Materials, 13(6), 329–341.
587 [4] Jefferis, S. (2012). Cement-Bentonite Slurry Systems. Grouting and Deep Mixing
588 2012, 1-24.
589 [5] Alzayani, N. J., Royal, A. C. D., Ghataora, G. S., & Jefferson, I. (2017). Cement-
590 bentonite in comparison with other cemented materials. Environmental Geotechnics,
591 4(5), 353–372.
592 [6] Joshi, K., Kechavarzi, C., Sutherland, K., Ng, M. Y. A., Soga, K., & Tedd, P. (2010).
593 Laboratory and In Situ Tests for Long-Term Hydraulic Conductivity of a Cement-
594 Bentonite Cutoff Wall. Journal of Geotechnical and Geoenvironmental Engineering,
595 136(4), 562-572.
596 [7] Royal, A. C. D., Opukumo, A. W., Qadr, C. S., Perkins, L. M., & Walenna, M. A.
597 (2018). Deformation and Compression Behaviour of a Cement–Bentonite Slurry for

598 Groundwater Control Applications. Geotechnical and Geological Engineering, 36(2),
599 835–853.
600 [8] Opdyke, S. M., & Evans, J. C. (2005). Slag-Cement-Bentonite Slurry Walls. Journal
601 of Geotechnical and Geoenvironmental Engineering, 131(6), 673–681.
602 [9] Cermak, Evans, & Tamaro. (2012). Evaluation of Soil-Cement-Bentonite Wall
603 Performance - Effects of Backfill Shrinkage. Grouting and Deep Mixing 2012, 502-511.
604 [10] Nejad, B. G., Osborne, T., & Carter, J. P. (2017). Forensic Investigation of a Slurry
605 Wall Failure: A Case Study. Grouting 2017, 513–522.
606 [11] Cao, B., Chen, J., & Al-Tabbaa, A. (2021). Crack-resistant cement–bentonite cut-
607 off wall materials incorporating superabsorbent polymers. Canadian Geotechnical
608 Journal, 58(6), 800-810.
609 [12] Alzayani, N. J. (2019). Impact of undrained deformation on the hydraulic
610 conductivity of cement-bentonite barrier material [PhD thesis, University of
611 Birmingham].
612 [13] Al-Tabbaa, A., & Harbottle, M. J. (2015). Self-healing materials and structures for
613 geotechnical and geo-environmental applications. Geotechnical Engineering for
614 Infrastructure and Development. 589-594.
615 [14] Reinhardt, H. W., & Jooss, M. (2003). Permeability and self-healing of cracked
616 concrete as a function of temperature and crack width. Cement and concrete research,
617 33(7), 981-985.
618 [15] Edvardsen, C. (1999). Water permeability and autogenous healing of cracks in

619 concrete. In Innovation in concrete structures: Design and construction (pp. 473-487).
620 Thomas Telford Publishing.
621 [16] De Rooij MR, Tittelboom K Van, De Belie N, Schlangen E (2013) Self-Healing
622 Phenomena in Cement-Based Materials: State-of-the-Art Report of RILEM Technical
623 Committee 221-SHC: Self-Healing Phenomena in Cement-Based Materials. Springer
624 [17] Liska, M., & Al-Tabbaa, A. (2008). Performance of magnesia cements in pressed
625 masonry units with natural aggregates: Production parameters optimisation.
626 Construction and Building Materials, 22(8), 1789–1797.
627 [18] Yi, Y., Liska, M., Akinyugha, A., Unluer, C., & Al-Tabbaa, A. (2013). Preliminary
628 Laboratory-Scale Model Auger Installation and Testing of Carbonated Soil-MgO
629 Columns. Geotechnical Testing Journal, 36(3), 20120052.
630 [19] Jin, F., & Al-Tabbaa, A. (2013). Thermogravimetric study on the hydration of
631 reactive magnesia and silica mixture at room temperature. Thermochimica acta, 566,
632 162-168.
633 [20] Qureshi, T. S., & Al-Tabbaa, A. (2016). Self-healing of drying shrinkage cracks in
634 cement-based materials incorporating reactive MgO. Smart Materials and Structures,
635 25(8), 084004.
636 [21] Alghamri, R., Kanellopoulos, A., Litina, C., & Al-Tabbaa, A. (2018). Preparation
637 and polymeric encapsulation of powder mineral pellets for self-healing cement based
638 materials. Construction and building Materials, 186, 247-262.
639 [22] Huang, X., Li, J. S., Guo, M. Z., Xue, Q., Du, Y. J., Wan, Y., & Poon, C. S. (2021).

Using MgO activated slag and calcium bentonite slurry to produce a novel vertical barrier material: Performances and mechanisms. Construction and Building Materials, 291, 123365.

[23] Sahamitmongkol, R., & Kishi, T. (2011). Tensile behavior of restrained expansive mortar and concrete. Cement and Concrete Composites, 33(1), 131-141.

[24] ASTM: D4219-08. (2008). Standard Test Method for Unconfined Compressive Strength Index of Chemical- Grouted Soils. ASTM International.

[25] ASTM: D5084-16. (2016). Standard Test Methods for Measurement of Hydraulic Conductivity of Saturated Porous Materials Using a Flexible Wall Permeameter. ASTM International.

[26] Wang, L., Chen, L., Provis, J. L., Tsang, D. C., & Poon, C. S. (2020). Accelerated carbonation of reactive MgO and Portland cement blends under flowing CO2 gas. Cement and Concrete Composites, 106, 103489.

[27] Alghamri, R., & Al-Tabbaa, A. (2020). Self-healing of cracks in mortars using novel PVA-coated pellets of different expansive agents. Construction and Building Materials, 254, 119254.

[28] Lee & Ryou. (2016). Crack Healing Performance of PVA-Coated Granules Made of Cement, CSA, and Na2CO3 in the Cement Matrix.

[29] Taylor, H. F. W., Barret, P., Brown, P. W., Double, D. D., Frohnsdorff, G., Johansen, V., Ménétrier-Sorrentino, D., Odler, I., Parrott, L. J., Pommersheim, J. M., Regourd, M., & Young, J. F. (1984). The hydration of tricalcium silicate. Materials and Structures,

661 17(6), 457–468.

662 [30] Wang, X., Fang, C., Li, D., Han, N., & Xing, F. (2018). A self-healing cementitious
663 composite with mineral admixtures and built-in carbonate. Cement and Concrete
664 Composites, 92, 216–229.

665 [31] Bureau of Reclamation. (2014). Design Standards No. 13: Embankment Dams.
666 Chapter 16. Cutoff Walls. United States.

667 [32] Evans, J. C., Larrahondo, J. M., & Yeboah, N. N. N. (2021). Fate of bentonite in
668 slag–cement–bentonite slurry trench cut-off walls for polluted sites. Environmental
669 Geotechnics, 40, 1-13.

670 [33] Wang, L., Chen, L., Provis, J. L., Tsang, D. C. W., & Poon, C. S. (2020).
671 Accelerated carbonation of reactive MgO and Portland cement blends under flowing
672 CO2 gas. Cement and Concrete Composites, 106, 103489.

673 [34] Scrivener, K., Snellings, R., & Lothenbach, B. (2018). A Practical Guide to
674 Microstructural Analysis of Cementitious Materials. CRC Press.

675 [35] Giannaros, P., Kanellopoulos, A., & Al-Tabbaa, A. (2016). Sealing of cracks in
676 cement using microencapsulated sodium silicate. Smart Materials and Structures, 25(8),
677 084005.

678 [36] Dung, N. T., & Unluer, C. (2016). Improving the performance of reactive MgO
679 cement-based concrete mixes. Construction and Building Materials, 126, 747–758.

680 [37] Giampouras, M., Garrido, C. J., Bach, W., Los, C., Fussmann, D., Monien, P., &
681 García-Ruiz, J. M. (2020). On the controls of mineral assemblages and textures in

682 alkaline springs, Samail Ophiolite, Oman. Chemical Geology, 533, 119435.

683 [38] Dung, N. T., & Unluer, C. (2018). Development of MgO concrete with enhanced

684 hydration and carbonation mechanisms. Cement and Concrete Research, 103, 160–169.

685 [39] Davies, P. J., & Bubela, B. (1973). The transformation of nesquehonite into

686 hydromagnesite. Chemical Geology, 12(4), 289–300.

687 [40] Liska, M., Vandeperre, L. J., & Al-Tabbaa, A. (2008). Influence of carbonation on

688 the properties of reactive magnesia cement-based pressed masonry units. Advances in

689 Cement Research, 20(2), 53–64.